



Physically mixed Ni₂Co/graphene catalyst for enhanced glucose oxidation in a glucose fuel cell

Yang Li¹ · Jie Ding¹ · Xianhua Liu¹ · Jiao Wang¹ · Shipu Jiao¹ · Ning Kang¹ · Jingyu Li¹ · Muhammad Irfan¹ · Pingping Zhang²

Received: 8 October 2021 / Revised: 24 December 2021 / Accepted: 3 January 2022 / Published online: 13 January 2022
© The Author(s), under exclusive licence to Springer-Verlag GmbH Germany, part of Springer Nature 2022

Abstract

Glucose oxidation reaction is kinetically sluggish and demands a highly efficient catalyst. Herein, we report a direct glucose alkaline fuel cell (DGAFC) using physically mixed Ni₂Co nanoparticles and reduced graphene oxide (Ni₂Co-rGO) supported on nickel foam as an anode to promote glucose oxidation. The DGAFC with the Ni₂Co-rGO anode delivered a remarkably enhanced peak power density of 40.44 W/m² at room temperature, which was 74.91% higher than the control (23.12 W/m²). Different techniques including XPS, SEM, linear sweep voltammetry, and electrochemical impedance spectroscopy were used to explore the physiochemical and electrochemical properties of the catalyst. Our results demonstrate that Ni₂Co-rGO exhibits an excellent activity toward glucose oxidation in alkaline medium, leading to a drastic improvement in the anode performance. There should be a synergistic effect between rGO and Ni₂Co. In the Ni₂Co-rGO nanocomposite, rGO not only acts as a support for the Ni₂Co nanoparticles and also promotes the electron transfer during the glucose oxidation process. This study can promote the development of bi-transition metal-based catalysts for DGAFCs.

Keywords Direct glucose alkaline fuel cell · Reduced graphene oxide · Non-noble metals · Anode

1 Introduction

The environmental pollution and diminishing conventional fuel sources make it more attractive for considering renewables as alternative energy sources. Fuel cells are electrochemical devices that convert chemical energy to electricity

and thermal energy. These systems are efficient, scalable to a wide range of sizes, environmentally friendly [1–4]. Although pure hydrogen is the most widely utilized substrate in fuel cells, its shortcomings such as hard storage and low production efficiency limit its large-scale application [5–7]. Biomass and biomass-derived fuels, such as ethanol, methanol, biodiesel, glycerol, and various carbohydrates, can be used directly or indirectly by fuel cell, representing one of the most promising energy supply systems in the future [8]. In the existing biomass-derived fuels, glucose is the most abundant monosaccharide in nature with an energy density of 4430 Wh/kg, which is even comparable to that of the most common substrate for direct fuel cell like methanol (6100 Wh/kg) [9, 10].

Glucose is categorized as a substrate into three main types of fuel cells based on the catalyst materials [11], including: microbial [12, 13], enzyme [14, 15], and abiotic fuel cells [16, 17]. Enzyme fuel cells are often applied in the field of miniaturization such as biosensors [18, 19]. Its main drawbacks are high cost and highly susceptible to environmental conditions [20–22]. Although microbial fuel cells do not easily being deactivated and poisoned, the slower speed and low efficiency of electron transfer from microorganisms to

Yang Li and Jie Ding contributed equally to this work

Highlights

- The catalyst has the advantages of low cost, easy fabrication and high efficiency.
- Maximum power density of 40.44 W/m² was obtained under ambient conditions.
- A synergistic effect between Ni₂Co and graphene was proposed.
- This study can facilitate the development of cost-effective catalysts for DGAFC.

✉ Xianhua Liu
lxh@tju.edu.cn

¹ School of Environmental Science and Engineering, Tianjin University, Tianjin 300354, People's Republic of China

² College of Food Science and Engineering, Tianjin Agricultural University, Tianjin 300384, People's Republic of China

electrodes lead to poor performance [23, 24]. Compared with microbial and enzymatic fuel cells, direct glucose alkaline fuel cell (DGAFC) has the advantages of strong durability, high stability, and simple structure.

In the existing metal catalysts for glucose oxidation, a variety of noble metals (Pd, Pt, Au, and Ag) have excellent performance. Basu et al. used NaBH_4 reduction technique to add Pd and Au with Pt precursor to form Pt–Pd–Au/C (metal ratio 1:1:1) catalyst that can efficiently electro-oxidize glucose in direct glucose fuel cell [25]. Rafaiideen et al. formed Pd/C by water-in-oil microemulsion [26]. Escalona-Villalpando et al. prepared Au-GO by electrodeposition to improve its oxidation performance to glucose [27]. However, the cost of noble metal catalyst is high and they are easily be poisoned by reaction intermediates, which hinders their practical application [16]. Recently, researchers found that NiCo composite catalysts exhibit good electrocatalytic activity for glucose oxidation. Gao et al. reported the fabrication of Ni–Co composite catalyst by using NaBH_4 reduction technique [28]. With it as the anode catalyst, the fuel cell can achieve 23.97 W/m^2 peak power density in 1 M glucose and 3 M KOH solution. Sarwar et al. prepared a Co–Ni/graphene catalyst by N_2H_4 reduction technique and tested its performance in a methanol fuel cell [29]. He found that increasing the concentration of nickel in Co–Ni/graphene can significantly promote the oxidation of methanol. Therefore, nickel and cobalt were used as catalyst precursors in this study for robust catalyst development.

Graphene has attracted significant attention due to its excellent properties. It demonstrated a certain electrocatalytic ability for redox reactions. More importantly, it has been proved to be an excellent supporting material to stabilize various electrocatalysts such as metal nanoparticles, metal oxides, and polymers [30, 31]. For example, Sun et al. used the technique of atomic layer deposition (ALD) to synthesize the monoatomic catalyst Pt/graphene, which improved the performance of the catalyst nearly ten times [32]. Baronia et al. used a graphene-based platinum-cobalt alloy catalyst prepared by chemical reduction to electrocatalytically oxidize methanol. It almost tripled the power density with respect to commercially available Pt/C catalyst [33]. It is suggested that graphene can play an important role both in the synthesis of metal catalysts and in its electrocatalytic process [34].

In this paper, a nickel–cobalt nanoparticle supported by reduced graphene oxide ($\text{Ni}_2\text{Co-rGO}$) was chemically synthesized and physically mixed as a catalyst for the glucose oxidation reaction. The thus-obtained composite catalyst demonstrated super performance than our previously developed catalysts based on transitional metals. Although tremendous work has been conducted on the fabrication of high-performance catalysts for glucose oxidation reaction, most of the fabrication processes need complex chemical

doping and group modification, which not only need sophisticated instruments, but also take time and effort. The ratio of transition metals to rGO was optimized. UV–Vis, Raman, XRD, XPS, and SEM were used to characterize the physicochemical and morphological properties of the catalyst. Electrochemical impedance spectroscopy (EIS), linear sweep voltammetry (LSV), power density, and polarization curve tests were used to evaluate the performance of the catalyst in DGAFC and unveil the possible underlying mechanism.

2 Experimental

2.1 Materials

Graphite powder (purity: 99.95%, mesh: 325) was purchased from Jinrilai Graphite Co. Ltd (Qingdao, China). A total of 60 wt% PTFE solution was provided by Heshen Inc. (Shanghai, China). Activated Carbon (AC) powder (YEC-8A) was obtained from Yihuan Carbon Co. Ltd (Fuzhou, China). Nickel foam was purchased from Liyuan New Material Co. Ltd (Changde, China) (purity: 99.9%, number of pores per inch: 110, density: 380 g/m^2 , average pore size: 590 nm, thickness: 1.7 mm). Glucose, $\text{NiSO}_4 \cdot 6\text{H}_2\text{O}$, $\text{Co}(\text{NO}_3)_2 \cdot 6\text{H}_2\text{O}$, NaBH_4 and other chemicals were all of the analytical grade. Deionized water (Millipore, Milli Q, 18.3 MU) was used to prepare all the solutions.

2.2 Preparation of Ni_2Co composite

Gao et al. have reported that the composite of nickel and cobalt had the best performance when Ni:Co = 2:1 [28]. Therefore, this ratio was directly used in this study without further optimization. The detailed procedure is as follows. A total of 500 mL of 0.04 M NiSO_4 and 0.02 M $\text{Co}(\text{NO}_3)_2$ was prepared in deionized water, and then, 0.15 g of citric acid was added. The solution was ultrasonically agitated for 10 min at $30 \text{ }^\circ\text{C}$, and then purged with nitrogen for 15 min. After that, 20 mL of 2 M sodium borohydride solution was drop wisely added with magnetic stirring and a black precipitate was formed. After 3 h, the black precipitate was washed with deionized water 3 to 5 times and vacuum dried at $50 \text{ }^\circ\text{C}$ for 12 h to obtain a powdery nickel–cobalt composite catalyst.

2.3 Preparation of reduced graphene oxide

GO was prepared via the modified Hummer's method (Preparation.S1) [35, 36]. Glucose was employed as a green reducing agent to produce rGO, which was also reported in various other studies [37, 38]. Take 40 mL of 7 mg/mL GO and dilute to 200 mL with deionized water and sonicate for 1 h. A total of 3.2 g of glucose was added to the diluted GO

solution, stirred magnetically for 30 min, and then 4 mL of ammonia was added and stirred for several minutes. The mixed solution was magnetically stirred in a 90 °C water bath for 1 h to form a black precipitate. The black precipitate was suction filtered with 500 mL of deionized water and freeze-dried to obtain rGO.

2.4 Fabrication of the Ni₂Co-rGO modified anode for DGAFC

The prepared graphene and nickel cobalt are mixed into the activated carbon, and loaded onto the foamed nickel by roll pressing, as shown in Fig. 1 [39]. Six experimental groups (rGO: Ni₂Co = 100:0/75:25/50:50/25:75/10:90/0:100) were set according to different mass ratios of rGO and Ni₂Co, and bare AC was used as the control group.

2.5 Electrochemical measurements

Electrochemical characterization is tested on electrochemical workstations, (CHI 660E, CHI Instrument Co. Ltd, Shanghai, China). Conventional three-electrode system was employed including a platinum sheet as the counter electrode, an Hg/HgO electrode as the reference electrode, and an anode used as the working electrode. LSV of all the anodes were tested from open circuit potential (OCP) to 0 V (vs Hg/HgO) with a scan rate of 1 mV/s. EIS of all the anodes were conducted over a frequency range of 100 kHz–10 MHz at the OCP, and the data was analyzed using ZSimpWin by fitting the EIS curve with an equivalent circuit. For cyclic voltammetry (CV) analysis, catalyst ink was prepared and coated onto the GCE as previously described [40]. The CV test was conducted under the

conditions of 3 M KOH and 1 M glucose solution, with a potential range of −0.7~0.1 V (vs Hg/HgO), and scan rate of 50 mV/s. The electrochemically active surface area (ECSA) of the catalyst is proportional to the electrochemical double-layer capacitance (C_{dl}). For C_{dl} , CV curves were measured at scan rates of 20, 40, 60, 80, and 100 mV/s in the non-Faradic region, and C_{dl} (mA/cm²) was obtained by plotting the current difference (Δj) relative to the scan rate. The ECSA (normalized by mass) was estimated by the following equation [41].

$$C_{dl} = d(\Delta j)/2dV_b \tag{1}$$

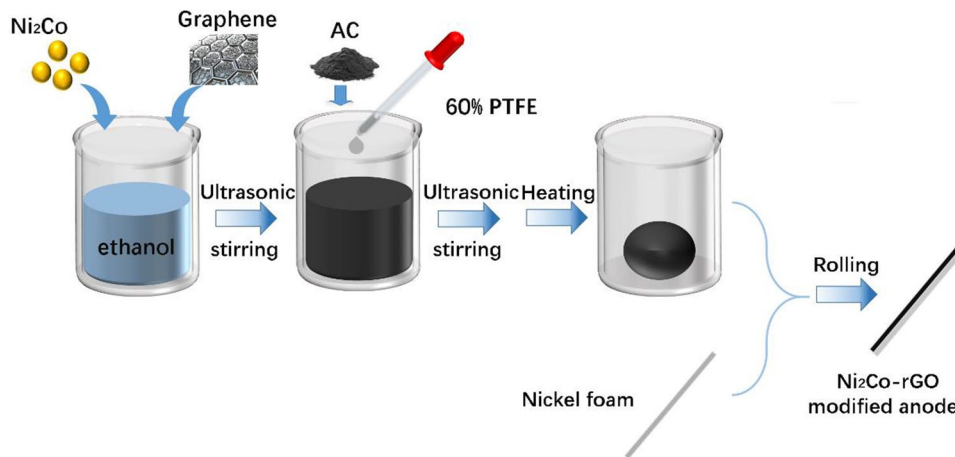
$$ECSA = C_{dl}/C_s \tag{2}$$

where C_{dl} refers to the double layer capacitance (mF) and V_b is the scan rate. ECSA denotes to the actual area of the working electrode (cm²), and C_s represents the specific capacitance of the catalyst (mF/cm²). C_{dl} was measured by CVs at the different scan rates of 20, 40, 60, 80, and 100 mV/s. The C_s generally refers to ~0.04 mF/cm² in 3 M KOH [42]. The power density and polarization curve of fuel cell were measured by external resistance method (Calculation.S2) [43].

2.6 Physical characterizations

Scanning electron microscope (SEM, HITACHI/S-4800) was used to investigate the morphology and specific surface area. Brucker D8 diffractometer was used to investigate X-ray diffraction (XRD) spectrum. X-ray photoelectron spectroscopy (XPS) spectra were with an Al K α radiation by Thermo Scientific Escalab 250Xi instrument. Raman spectrometer (the RM2000 from Renishaw in the UK) was used for the characterization of nanocomposites.

Fig. 1 Fabrication of the Ni₂Co-rGO modified anode for DGAFC



3 Results and discussions

3.1 Electrochemical performance of Ni₂Co-rGO anode in DGAFC

As shown in Fig. 2A, according to the slope of the LSV polarization curve, the experimental groups were significantly better than the control group, and the performance of 25 mg rGO + 75 mg Ni₂Co group was the best. At the same time, when the anode potential is -0.4 V (vs Hg/HgO), the current density of the optimal group is as high as 24.57 mA/cm², 35% higher than the Bare/AC (18.2 mA/cm²), and 4.53 mA/cm² higher than the 100 mg rGO, 2.18 mA/cm² higher than the 100 mg Ni₂Co, indicating that both catalysts play a significant role in promoting glucose oxidation and that there may be synergies between the two. The ligand effect improved the electronic structure of the bimetallic catalyst, whereas the strain effect modified the electronic structure by varying the orbital overlap. Second, adding rGO increased its electrical conductivity, catalytic capacity for glucose oxidation, and current density. For an anode with only graphene and Ni₂Co catalysts, although both have a certain amount of electrocatalytic performance, the current density of Ni₂Co is still significantly higher than that of graphene.

After comparing the respective and common catalysis of nickel–cobalt graphene in Fig. 2A, the ratio between Ni₂Co and rGO was adjusted in Fig. 2B for comparison. Figure 2B shows that the anode performance increased with the addition of Ni₂Co. And when the amount added

exceeded 75 mg (: 1 g AC), the performance decreased. This proved that a smaller amount of graphene could improve its performance effectively. And when its content was too high, it will impair the performance of Ni₂Co. At the same time, compared with the blank group, the higher open circuit voltage also proved its performance improvement on the other hand.

Unlike LSV, EIS evaluates electrode performance by obtaining information about electrode reaction kinetics and electrode interface structure by measuring impedance changes over a wide frequency range. Figure 3 shows the Nyquist plot of all anodes treated by the equivalent circuit method. In the above equivalent circuit, the total resistance is composed of five parts, diffusion resistance (R_d), pore adsorption capacitance (C_{ad}), charge transfer resistance (R_{ct}), layer capacitance (C_{dl}), and ohmic resistance (R_s). The variation of each anode resistance is reflected in Table 1 and Fig. 3.

It can be seen from Table 1 that whether it is R_s , R_{ct} , R_d , or R_p , these characteristics of the electrode to which the catalyst is added are significantly improved. The relationship between the four is that R_p is the sum of R_s , R_{ct} , and R_d . From the R_p point of view, the R_p variation of each experimental group is consistent with the law shown by LSV. In Table 1 and Fig. 3B, the R_p of the blank group (3.3814 Ω) is 2.13 times that of 25 mg rGO + 75 mg Ni₂Co (1.0805 Ω), 1.36 times that of 100 mg rGO (1.4349 Ω), and 1.45 times that of 100 mg Ni₂Co (1.3778 Ω). The order of display of the experimental group in which rGO and Ni₂Co are mixed in different ratios is: 25 mg rGO + 75 mg Ni₂Co (1.0805 Ω) < 50 mg rGO + 50 mg Ni₂Co (1.2508 Ω) < 10 mg

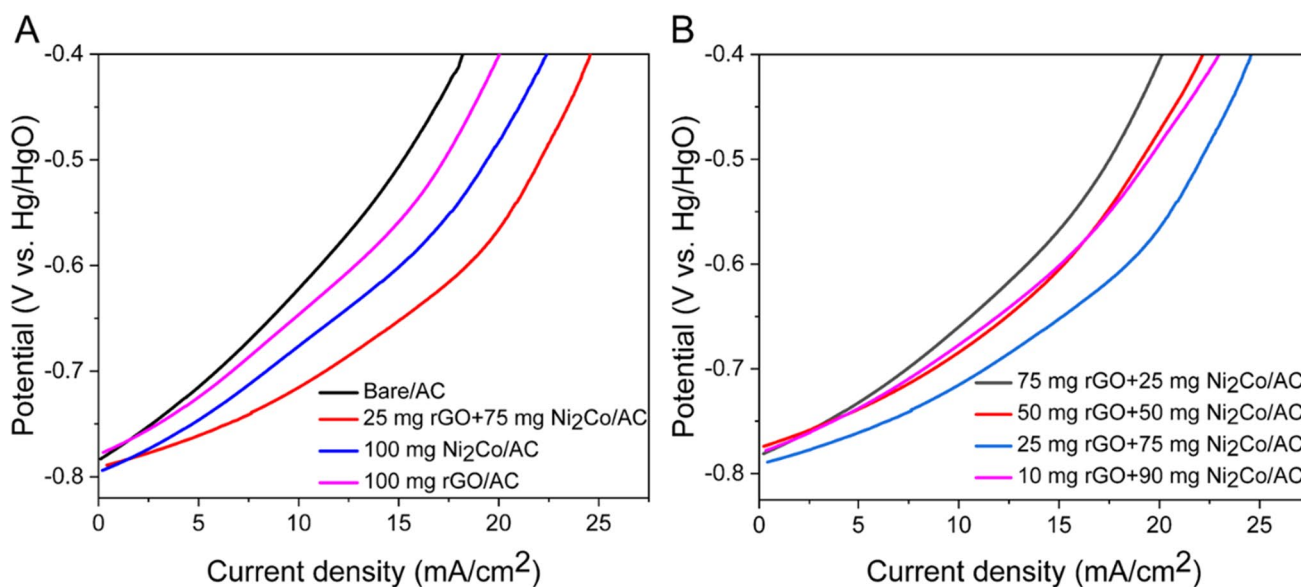


Fig. 2 **A** LSV polarization curves for the electrodes with bare AC, Ni₂Co/AC, rGO/AC, and Ni₂Co-rGO/AC. **B** LSV polarization curves for the anodes with different ratio between Ni₂Co and rGO

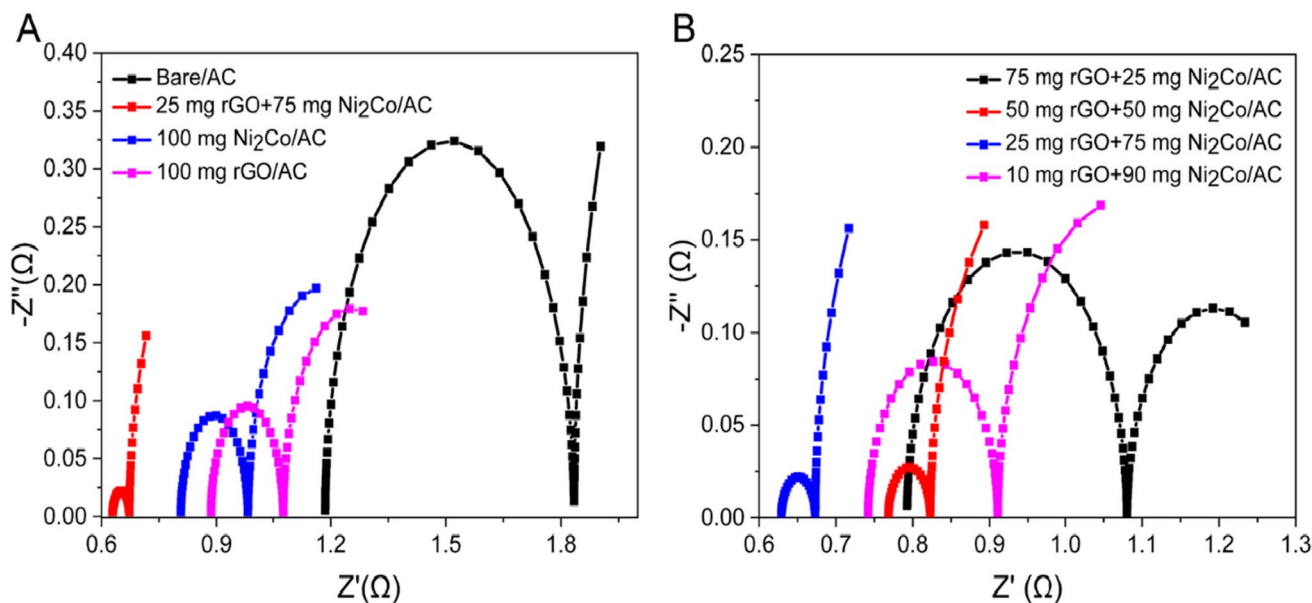


Fig. 3 **A** Nyquist plots of EIS for the anodes with bare AC, Ni₂Co/AC, rGO/AC, and Ni₂Co-rGO/AC. **B** Nyquist plots of EIS for the anodes with different ratio between Ni₂Co and rGO

Table 1 Fitting results of different anodes based on the equivalent circuit

	R_s (Ω)	C_{ad} (F)	R_{ct} (Ω)	C_{dl} (F)	R_d (Ω)	R_t (Ω)
Bare AC	1.186	0.00035	0.6484	3.239	1.5470	3.3814
100 mg rGO	0.8855	0.00181	0.1906	37.82	0.3588	1.4349
100 mg Ni ₂ Co	0.8069	0.00154	0.1748	73.90	0.3961	1.3778
25 mg rGO + 75 mg Ni ₂ Co	0.6289	0.04535	0.0441	94.31	0.4075	1.0805
10 mg rGO + 90 mg Ni ₂ Co	0.7419	0.00362	0.3453	57.45	0.1687	1.2559
50 mg rGO + 50 mg Ni ₂ Co	0.7683	0.03455	0.0549	84.09	0.4276	1.2508
75 mg rGO + 25 mg Ni ₂ Co	0.7925	0.00028	0.2876	48.39	0.2261	1.3061

rGO + 90 mg Ni₂Co (1.2559 Ω) < 75 mg rGO + 25 mg Ni₂Co (1.3061 Ω) < 100 mg Ni₂Co (1.3778 Ω) < 100 mg rGO (1.4349 Ω) < Bare AC (3.3814 Ω). According to the obtained results, it is apparent that the addition of Ni₂Co-rGO can significantly facilitate the electrons transfer process by the reduction of R_t . These results are highly consistent with LSV.

It can be seen from Table 1 that the trend of R_s is completely consistent with R_t , which is R_s of 25 mg rGO + 75 mg Ni₂Co and 46.97% of that of the blank group. The R_{ct} and R_d of the experimental group were optimized from different directions, although they were different from the trend of R_t . In the end, 25 mg of R_{ct} decreased by 93.19%, and R_d decreased by 73.66%, compared to Bare/AC. From this point of view, the most important effect in reducing R_t is the reduction of R_{ct} . R_{ct} represents the resistance of the thin liquid film in the pore structure of the activated carbon layer to the transfer of electrolyte ions and internal charges. It can be seen that the addition of rGO and Ni₂Co gives the electrode a faster electron transfer rate.

The influence of the scan rate on glucose oxidation was further determined by using CV (Fig. 4A–B). CV of Ni₂Co-rGO was performed by varying scan rates from 20 to 100 mV/s. The oxidation peak current was increased by increasing the scan rate as demonstrated in Fig. 4A. Figure 4B shows the linearity in the anodic current peak of all the catalysts versus square roots of the scan rate, revealing that the electrochemical oxidation of glucose is a diffusion-controlled process [44].

The C_{dl} was calculated by CV curves at different scanning rates, and the corresponding fitting lines of 3 samples plotted by capacitive currents versus scan rates were shown in Fig. 4C. Ni₂Co-rGO/AC exhibited higher ECSA (~98.0 m²/g) than Ni₂Co/AC (~86.0 m²/g) and rGO/AC (~67.8 m²/g). A higher ECSA value means that there is a larger contact area between the electrocatalyst surface and the electrolyte, which makes a positive effect on electrocatalysis, indicating the composite catalyst of Ni₂Co-rGO has more active reaction sites.

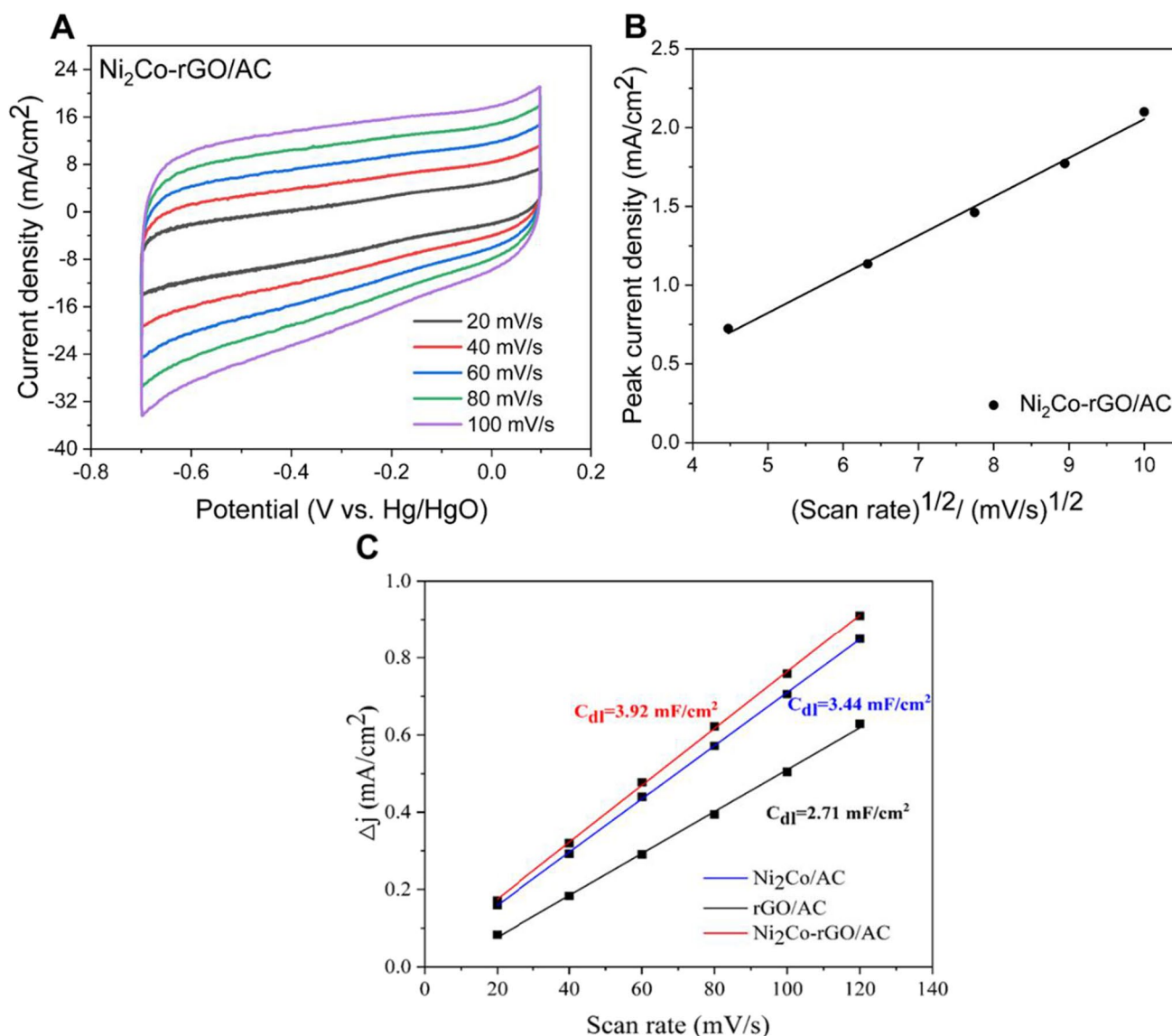


Fig. 4 **A** CV curves for Ni₂Co-rGO/AC at scan rates of 20 mV/s, 40 mV/s, 60 mV/s, 80 mV/s, and 100 mV/s in 1 M Glucose and 3 M KOH media. **B** Plot of anodic peak currents versus the square root of scan rate. **C** Scan rate dependence of the current densities

The previous tests on EIS and LSV were for half-cell tests. After the same cathodes were assembled with the above anodes, the subsequent power density curves (Fig. 5A) and anode/cathode polarization curves were tested (Fig. 5B). Figure 5 shows that the best performance of the 25 mg rGO + 75 mg Ni₂Co group is still the most prominent among the power density and anodic polarization curves. Its maximum power density (40.44 W/m²) is 74.91% higher than the blank group (23.12 W/m²), 35.89% higher than the 100 mg rGO group (29.76 W/m²), and 29.87% higher than the 100 mg Ni₂Co group (31.14 W/m²). In the case of a very close cathodic polarization curve, the changing trend of the anode polarization curve whose peak value is 105.1 A/m² (Bare AC) < 115.88 A/m² (rGO) < 123.64 A/

m² (Ni₂Co) < 143.84 A/m² (Ni₂Co-rGO) confirms that the change of the power density curve is caused by the improvement of the performance of the anode.

3.2 Physical characterization of electrode

UV–vis absorption spectroscopy is used here first to monitor the synthesis of GO and rGO. In Fig. 6, the graphite solution was detected to have only one horizontal line, and the GO solution after the hummer treatment showed a distinct peak at 230 nm and 300 nm. This proves that the hummer method successfully converts C–C in graphite into C=C double bond and C=O double bond in GO. Otherwise, in Fig. 6A, as the concentration of GO increases, the peaks of

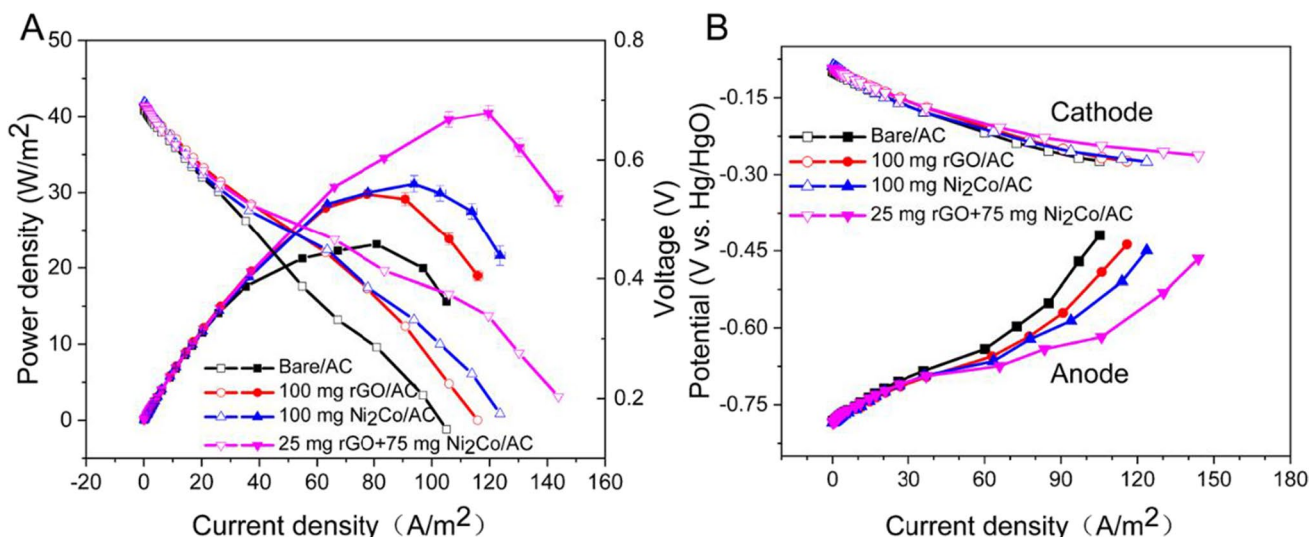


Fig. 5 Power density curves (A) and polarization curves (B) of DGAFs equipped with different anodes

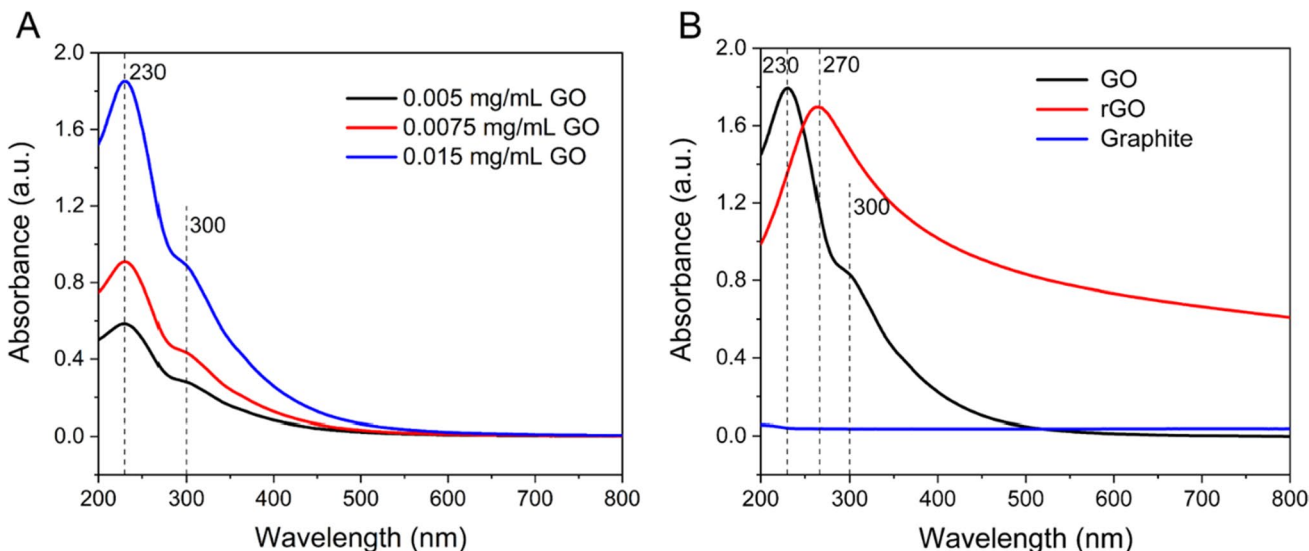


Fig. 6 A UV-vis absorption spectra collected GO with different concentrations. B UV-vis absorption spectra collected GO, rGO, and graphite

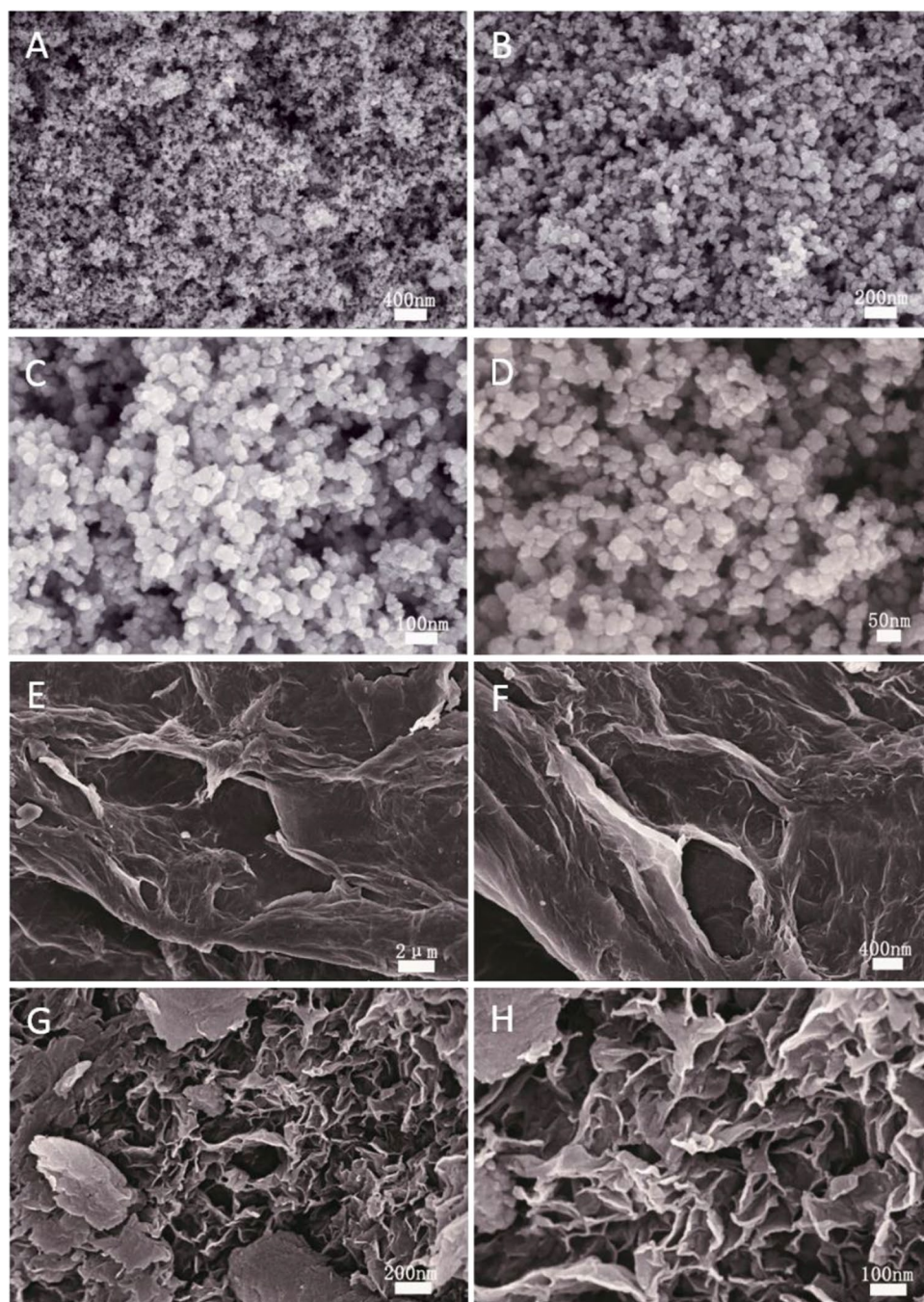
both peaks increase in a certain gradient, indicating that GO is dispersed uniformly in aqueous solution, and there is no obvious impurity [28].

Then, the graphene reduced with glucose was centrifuged and washed to prepare a suspension, which was tested in UV-vis to obtain the curve in Fig. 6B. The peak appearing at 300 nm in this curve is the GO being reduced. During the disappearance of the oxygen-containing functional group, the sp^2 electron conjugated bond was restored and a new lattice was formed [45]. In brief, under the monitoring of UV-vis, it is very smooth from graphite to GO to rGO.

Figure 7 is SEM images of nickel-cobalt alloy and graphene in the catalyst, respectively. Figure 7A–D shows that

the nickel-cobalt material is uniformly distributed in a nano-spherical shape with a diameter of about 20 nm, and the diameter of the nickel-cobalt is reduced by 60% compared with the diameter of the nickel material alone [28]. The characteristics of these surfaces indicate that the nickel-cobalt material can be well dispersed with graphene and activated carbon. Additionally, the composite has a comparable network structure and many linked channels, which helps ions diffuse from the bulk solution to the porous material inner surface. These reactions created a large amount of free space and electroactive surface sites; both metals size and atomic weight are nearly same, which may cause ionic contact between Ni and Co. This sympathetic structure may increase

Fig. 7 SEM images of Ni₂Co nanocomposite (A–D) and rGO (E–H)



surface contact with the substrate, promote substrate mass movement inside the dynamic material, and improve electrochemical performance.

The electron micrograph of the graphene powder reduced by glucose is shown in Fig. 7E–H, and the graphene has a multi-pleated and multi-pleated sheet structure. The graphene under the electron microscope is like a peony flower, and the layered structure of graphene is the petal of the peony flower. This structure causes graphene to hold a large number of electrons and ions or even amorphous

nickel–cobalt particles, thereby promoting the mass transfer process. The SEM and corresponding elemental mapping images of the Ni₂Co-rGO display the uniform dispersion of O, Co, and Ni (Fig. 8A–E).

The XRD profile of Ni₂Co-rGO is shown in Fig. 8F. Three sharp peaks ($2\theta = \sim 13^\circ/16^\circ/27^\circ$) were found in the XRD pattern of Ni₂Co-rGO. The peaks indexed at $\sim 27^\circ$ signify the crystalline structure of graphite [46, 47]. Meanwhile, the peaks of GO and rGO are at $\sim 10^\circ$ [38, 46, 47]. So the peak ($2\theta = \sim 13^\circ$) means that GO or rGO may exist.

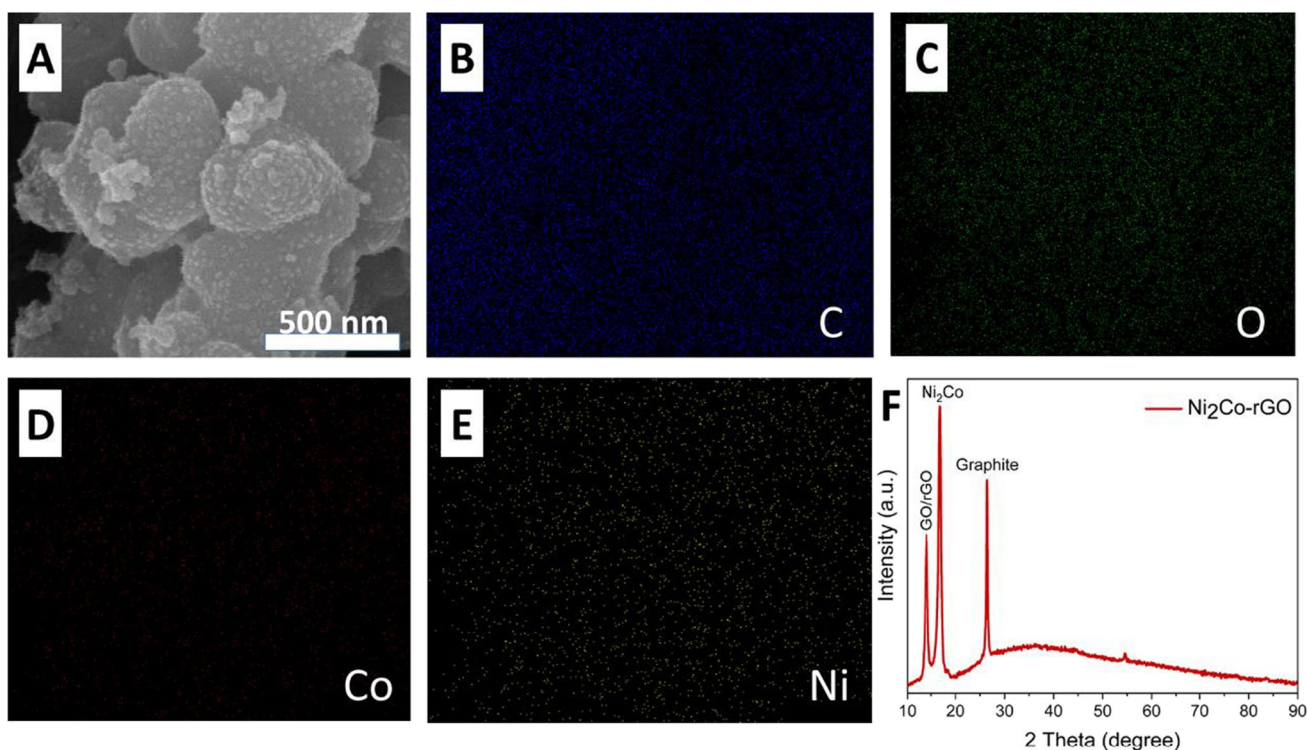


Fig. 8 Structural and elemental analyses of Ni₂Co-rGO. **A** SEM image of Ni₂Co-rGO. **B–E** Corresponding element mapping of C, O, Co, and Ni. **F** XRD patterns of Ni₂Co-rGO catalysts

And the peak ($2\theta = \sim 16^\circ$) is a typical diffraction peak of NiCo [48, 49].

To further study the morphology of the catalyst, the activated carbon was physically mixed with the catalyst, and XPS was used to indicate the surface structure of the catalyst. Since this XPS test was performed after the catalyst was mixed with activated carbon, the nickel–cobalt noise was relatively large, but the approximate morphology could be distinguished. First, in Fig. 9A, the XPS of C 1s shows the carbon elements with different energies in different states in the test sample. There are 284.2 eV (C–C), 286.1 eV (C–O), 273.3 eV (C=O), and 289 eV (O–C=O). It can be seen that the oxygen-containing functional groups in the graphene in the catalyst still have some residual, but the content is not high and does not affect the properties of the graphene itself.

While Fig. 9B and C are the XPS results of Co 2p and Ni 2p in the catalyst, respectively, both elements have detected different binding energies, which indicates that there is more than one form of nickel and cobalt present in the catalyst. In the XPS diagram of nickel, the peak of Ni 2p_{3/2} is about 855.9 eV and the peak of Ni 2p_{1/2} is 873.9 eV, which is attributed to Ni³⁺ of NiOOH. Adjacent, the peak of Ni 2p_{3/2} is about 857.6 eV and the peak of Ni 2p_{2/1} is 875.65 eV, which corresponds to Ni²⁺ in Ni(OH)₂. The other four Ni 2p_{1/2} and Ni 2p_{3/2} peaks in the figure are the satellite peaks of NiOOH and Ni(OH)₂ described above. Concerning

the XPS image of cobalt in Fig. 9C, there are two peaks of 783.8 eV and 786.2 eV in the Co 2p_{3/2} portion and two peaks of 798.8 eV and 801.2 eV corresponding to the Co 2p_{1/2} portion. The remaining four peaks in the picture are satellites. These are the characteristics of divalent cobalt. At last, according to the results of fitting the XPS data on the Avantage software, the nickel element mass accounts for 60.39% of the total amount of nickel and cobalt.

In addition to UV, Raman is also used to detect the internal structural characteristics of the material. In addition, Raman can provide different information such as the number of layers of material structure. As shown in Fig. 9D, very distinct G-bands and D-bands appear at 1584 cm⁻¹ and 1344 cm⁻¹, which represent sp² carbon in the plane and sp³ carbon in the out-of-plane vibration, respectively [50]. It is also shown from the literature that the ratio of the intensity of the D band to the G band is the key to distinguishing the state of the graphene, and the $I_D/I_G > 1$ in the figure indicates that the graphite in the material has been converted into graphene [51, 52]. For the nickel element, two related broad peaks appear in the figure, which are 1064 cm⁻¹ and 512 cm⁻¹ respectively. According to the literature, the longer wavelength represents the presence of Ni⁰, and the shorter wavelength is mainly the performance of Ni₂O₃. On the other hand, the peak ratio of the two places indicates that the form of

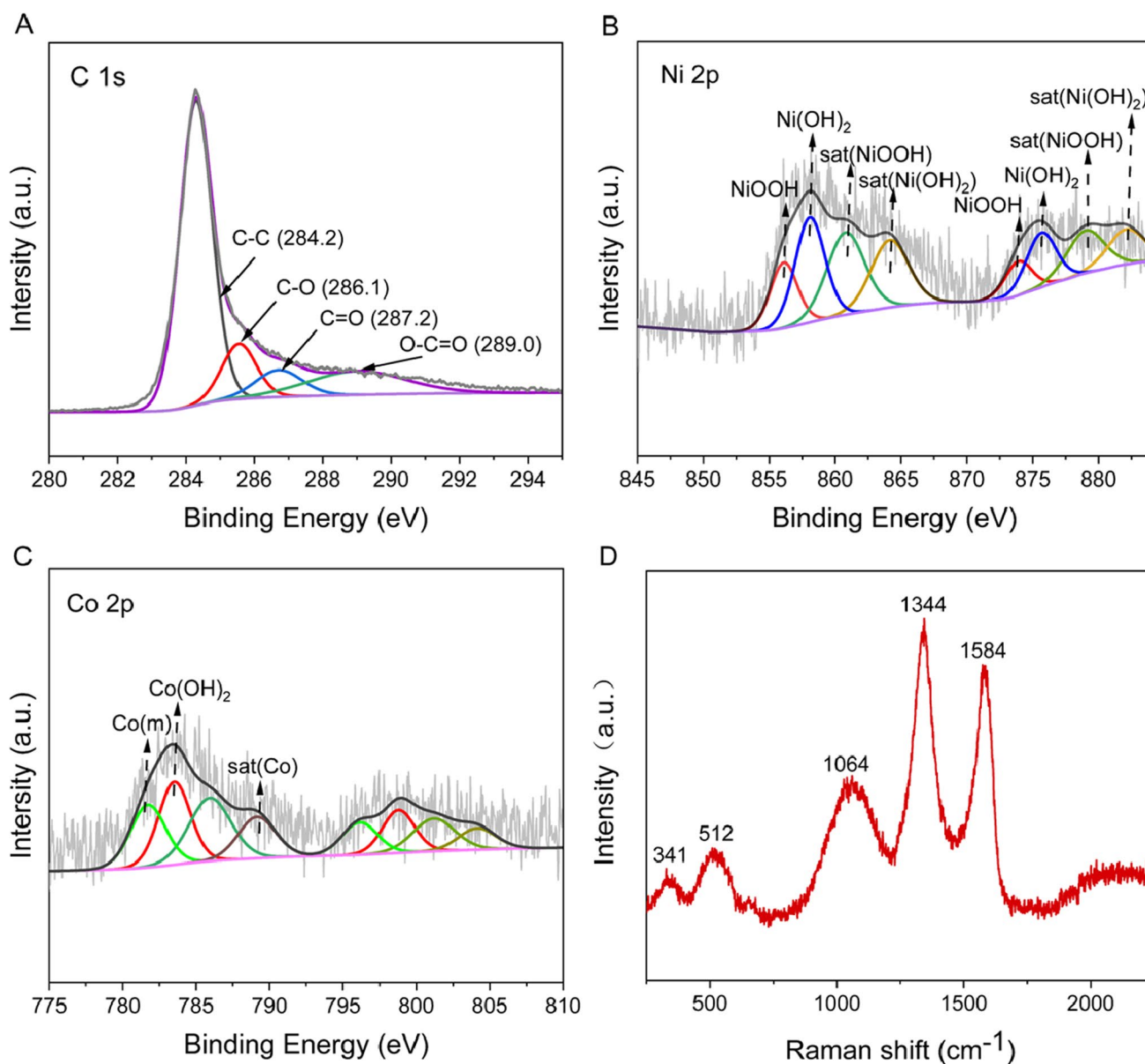
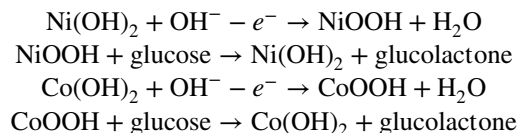


Fig. 9 The C 1 s (A), Ni 2p (B), and Co 2p (C) XPS spectra of Ni₂Co-rGO. Raman of Ni₂Co-rGO(D)

nickel in the material is mainly Ni⁰. The last remaining weak broad peak 341 cm⁻¹ proves the presence of cobalt.

3.3 Catalytic mechanism of Ni₂Co-rGO

In the Ni₂Co-graphene catalyst, the catalytic action of nickel–cobalt mainly comes from the process of electron transfer generated by the process of converting into the respective hydroxide under alkaline conditions. The process is as follows:



What occurs mainly at the anode of the DGAFc is the process of electrochemical oxidation of glucose, but this process is significantly inhibited by the process of electron transfer, and the key to improving efficiency is to ensure that the reaction of glucose with OH⁻ is sufficient and efficient. The above four reaction equations indicate that nickel–cobalt

Table 2 Performance parameters of different anode catalysts for various DGAFCS

Anode catalyst	P_{\max} (W/m ²)	OCV (V)	Glucose (M)	Membrane	T (°C)	Ref
Au/Ni-foam	226.0	0.83	0.5	Yes	70	[54]
FCO-AC	35.9	0.79	1.0	No	25	[39]
Pt/rGO	10.8	0.94	0.05	Yes	25	[55]
NiCo-AC	24.0	0.80	1.0	No	25	[28]
Carbon fiber	14.5	0.80	0.4	Yes	25	[56]
Ag	20.3	0.59	1	Yes	80	[57]
Ni ₂ Co-rGO/AC	40.4	0.73	1.0	No	25	This work

oxidation at the anode is mainly dependent on the two redox pairs of Ni(II)/Ni(III), Co(II)/Co(III). It represents a process in which both Ni(II) and Co(III) can combine with OH⁻ to form NiOOH and CoOOH under alkaline conditions and release electrons. NiOOH and CoOOH participate in the reverse reaction while converting glucose to glucolactone.

Simultaneously, there should be a synergy between the two pairs of reversible reactions. Among them, nickel is believed to play a main role in the electrocatalytic oxidation of glucose; however, the presence of cobalt is crucial to help form a nanoscale composite and create more active sites. As to rGO, high conductivity, outstanding charge carrier rates, large surface area, and unique two-dimensional structure make it good support for metal catalysts [53]. Therefore, these characteristics allow rGO to remarkably promote the activity of nickel and cobalt for the glucose oxidation reaction. These results suggested that the Ni₂Co-graphene composite are electrocatalytically active and stable for glucose oxidation, and applicable for prospect energy devices.

Table 2 is a summary of recently reported anodic catalysts for direct glucose fuel cells. The data of this work are also displayed. These results revealed that the composite catalyst of Ni₂Co-rGO would dramatically enhance its electrochemical performance.

4 Conclusion

Fabrication of composite catalysts usually involves complex chemical doping and group modification, which not only takes time and effort, and increases the product cost. In this study, a high efficient composite catalyst, Ni₂Co-rGO, was prepared by using a simple physically mixing method, which greatly boosts the catalytic oxidation glucose in a DGAFCS. When rGO:Ni₂Co = 2.5:7.5, the catalyst achieved the highest efficiency under room temperature, and its power density reached 40.44 W/m², which was 74.91% higher than the control (23.12 W/m²). The excellent performance of Ni₂Co-rGO came not only from the excellent catalytic ability of nickel and cobalt, but also from their synergistic effect with rGO, which had the fluffy porous structure and excellent conductivity. This low-cost non-noble metal combination has great

potential to replace noble metal catalysts such as platinum in the future development of DGAFCS.

Supplementary Information The online version contains supplementary material available at <https://doi.org/10.1007/s13399-022-02317-3>.

Funding This work was partially supported by the National Key R&D Program of China (Grant No. 2019YFC1407800) and the Natural Science Foundation of Tianjin City (Grant No. 19YFZCSN01130).

Declarations

Conflict of interest The authors declare no competing interests.

References

- Wang Y, Diaz DFR, Chen KS, Wang Z, Adroher XC (2020) Materials, technological status, and fundamentals of PEM fuel cells—a review. *Materials today* 32:178–203
- Pan Z, An L, Zhao T, Tang Z (2018) Advances and challenges in alkaline anion exchange membrane fuel cells. *Prog Energy Combust Sci* 66:141–175
- Wang J, Wang H, Fan Y (2018) Techno-economic challenges of fuel cell commercialization. *Engineering* 4(3):352–360
- Wilberforce T, Ijaodola O, Ogungbemi E, Khatib F, Leslie T, El-Hassan Z, Thomposon J, Olabi A (2019) Technical evaluation of proton exchange membrane (PEM) fuel cell performance—a review of the effects of bipolar plates coating. *Renewable and Sustainable Energy Reviews*. 113:109286
- Alias M, Kamarudin S, Zainoodin A, Masdar M (2020) Active direct methanol fuel cell: an overview. *Int J Hydrog Energy* 45(38):19620–19641
- Hao W, Ma H, Sun G, Li Z (2019) Magnesia phosphate cement composite bipolar plates for passive type direct methanol fuel cells. *Energy* 168:80–87
- Zakaria Z, Kamarudin SK (2016) Direct conversion technologies of methane to methanol: an overview. *Renew Sustain Energy Rev* 65:250–261
- Mohammed H, Al-Othman A, Nancarrow P, Tawalbeh M, El Haj AM (2019) Direct hydrocarbon fuel cells: a promising technology for improving energy efficiency. *Energy* 172:207–219
- Leo TJ, Raso MA, Navarro E, Mora E (2013) Long term performance study of a direct methanol fuel cell fed with alcohol blends. *Energies* 6(1):282–293
- Fujiwara N, Yamazaki S-i, Siroma Z, Ioroi T, Senoh H, Yasuda K (2009) Nonenzymatic glucose fuel cells with an anion exchange membrane as an electrolyte. *Electrochemistry communications* 11(2):390–392

11. Toriogoe K, Takahashi M, Tsuchiya K, Iwabata K, Ichihashi T, Sakaguchi K, Sugawara F, Abe M (2018) High-power abiotic direct glucose fuel cell using a gold–platinum bimetallic anode catalyst. *ACS omega* 3(12):18323–18333
12. Lawson K, Rossi R, Regan JM, Logan BE (2020) Impact of cathodic electron acceptor on microbial fuel cell internal resistance. *Bioresource technology*. 316:123919
13. Silveira G, de Aquino Neto S, Schneedorf JM (2020) Development, characterization and application of a low-cost single chamber microbial fuel cell based on hydraulic couplers. *Energy*. 208:118395
14. Sorrentino I, Gentil S, Nedellec Y, Cosnier S, Piscitelli A, Giardina P, Le Goff A (2019) POXC laccase from pleurotus ostreatus: a high-performance multicopper enzyme for direct oxygen reduction reaction operating in a proton-exchange membrane fuel cell. *ChemElectroChem*. 6(4):1023–1027
15. Cracknell JA, Vincent KA, Armstrong FA (2008) Enzymes as working or inspirational electrocatalysts for fuel cells and electrolysis. *Chemical Reviews*. 108(7):2439–2461
16. Ahmad YH, Mohamed AT, El-Shafei A, Al-Qaradawi SY, Aljaber AS (2020) Facile one-step synthesis of supportless porous AuPtPd nanocrystals as high performance electrocatalyst for glucose oxidation reaction. *International Journal of Hydrogen Energy*. 45(38):19163–19173
17. Xu H, Yan B, Zhang K, Wang J, Li S, Wang C, Du Y, Yang P, Jiang S, Song S (2017) N-doped graphene-supported binary PdBi networks for formic acid oxidation. *Appl Surf Sci* 416:191–199
18. Huang J, Zhao P, Jin X, Wang Y, Yuan H, Zhu X (2020) Enzymatic biofuel cells based on protein engineering: recent advances and future prospects. *Biomaterials science* 8(19):5230–5240
19. Xiao X, Xia H-q, Wu R, Bai L, Yan L, Magner E, Cosnier S, Lojou E, Zhu Z, Liu A (2019) Tackling the challenges of enzymatic (bio) fuel cells. *Chemical reviews* 119(16):9509–9558
20. Irfan M, Liu X, Li S, Khan IU, Li Y, Wang J, Wang X, Du X, Wang G, Zhang P (2020) High-performance glucose fuel cell with bimetallic Ni–Co composite anchored on reduced graphene oxide as anode catalyst. *Renewable Energy* 155:1118–1126
21. Frei M, Martin J, Kindler S, Cristiano G, Zengerle R, Kerzenmacher S (2018) Power supply for electronic contact lenses: abiotic glucose fuel cells vs. Mg/Air batteries *Journal of Power Sources* 401:403–414
22. Le PG, Kim MI (2021) Research progress and prospects of nanozyme-based glucose biofuel cells. *Nanomaterials* 11(8):2116
23. Bahari M, Malmberg MA, Brown DM, Nazari SH, Lewis RS, Watt GD, Harb JN (2020) Oxidation efficiency of glucose using viologen mediators for glucose fuel cell applications with non-precious anodes. *Applied Energy* 261:114382
24. Barzi S, Zhiani M, Ahmadi A (2019) Evaluation of carbon supported Fe–Co electrocatalyst for selective oxygen reduction to use in implantable glucose fuel cell. *International Journal of Hydrogen Energy* 44(59):31515–31524
25. Basu D, Basu S (2012) Performance studies of Pd–Pt and Pt–Pd–Au catalyst for electro-oxidation of glucose in direct glucose fuel cell. *International journal of hydrogen energy* 37(5):4678–4684
26. Rafaiideen T, Baranton S, Coutanceau C (2019) Highly efficient and selective electrooxidation of glucose and xylose in alkaline medium at carbon supported alloyed PdAu nanocatalysts. *Appl Catal B* 243:641–656
27. Escalona-Villalpando R, Gurrola M, Trejo G, Guerra-Balcázar M, Ledesma-García J, Arriaga L (2018) Electrodeposition of gold on oxidized and reduced graphite surfaces and its influence on glucose oxidation. *J Electroanal Chem* 816:92–98
28. Gao M, Liu X, Irfan M, Shi J, Wang X, Zhang P (2018) Nickel-cobalt composite catalyst-modified activated carbon anode for direct glucose alkaline fuel cell. *International Journal of Hydrogen Energy* 43(3):1805–1815
29. Sarwar E, Noor T, Iqbal N, Mehmood Y, Ahmed S, Mehek R (2018) Effect of Co-Ni ratio in graphene based bimetallic electrocatalyst for methanol oxidation. *Fuel Cells* 18(2):189–194
30. Yan Z, Xu Z, Yang Z, Yue L, Huang L (2019) Graphene oxide/Fe₂O₃ nanoplates supported Pt for enhanced room-temperature oxidation of formaldehyde. *Appl Surf Sci* 467–468:277–285
31. Han J, Jun B-M, Heo J, Lee G, Yoon Y, Park CM (2019) Highly efficient organic dye removal from waters by magnetically recoverable La₂O₂CO₃/ZnFe₂O₄-reduced graphene oxide nanohybrid. *Ceramics International* 45(15):19247–19256
32. Sun S, Zhang G, Gauquelin N, Chen N, Zhou J, Yang S, Chen W, Meng X, Geng D, Banis MN (2013) Single-atom catalysis using Pt/graphene achieved through atomic layer deposition. *Scientific Reports* 3(1):1–9
33. Baronia R, Goel J, Tiwari S, Singh P, Singh D, Singh SP, Singhal SK (2017) Efficient electro-oxidation of methanol using PtCo nanocatalysts supported reduced graphene oxide matrix as anode for DMFC. *International Journal of Hydrogen Energy* 42(15):10238–10247
34. Liu J, Choi HJ, Meng L-Y (2018) A review of approaches for the design of high-performance metal/graphene electrocatalysts for fuel cell applications. *J Ind Eng Chem* 64:1–15
35. Hummers WS Jr, Offeman RE (1958) Preparation of graphitic oxide. *Journal of the american chemical society* 80(6):1339–1339
36. Wang H, Wang G, Ling Y, Qian F, Song Y, Lu X, Chen S, Tong Y, Li Y (2013) High power density microbial fuel cell with flexible 3D graphene–nickel foam as anode. *Nanoscale* 5(21):10283–10290
37. Akhavan O, Ghaderi E, Aghayee S, Fereydooni Y, Talebi A (2012) The use of a glucose-reduced graphene oxide suspension for photothermal cancer therapy. *Journal of Materials Chemistry* 22(27):13773–13781
38. Sharma K, Maiti K, Kim NH, Hui D, Lee JH (2018) Green synthesis of glucose-reduced graphene oxide supported Ag–Cu₂O nanocomposites for the enhanced visible-light photocatalytic activity. *Compos B Eng* 138:35–44
39. Dong F, Liu X, Irfan M, Yang L, Li S, Ding J, Li Y, Khan IU, Zhang P (2019) Macaroon-like FeCo₂O₄ modified activated carbon anode for enhancing power generation in direct glucose fuel cell. *International Journal of Hydrogen Energy* 44(16):8178–8187
40. Yang L, Liu X, Ding J, Li S, Dong F, Irfan M, Li Y, Wang G, Du X, Zhang P (2019) Chlorella-derived porous heteroatom-doped carbons as robust catalysts for oxygen reduction reaction in direct glucose alkaline fuel cell. *International Journal of Hydrogen Energy* 44(5):2823–2831
41. Ho J, Li Y, Dai Y, Kim T, Wang J, Ren J, Yun H, Liu X (2021) Ionothermal synthesis of N-doped carbon supported CoMn₂O₄ nanoparticles as ORR catalyst in direct glucose alkaline fuel cell. *International Journal of Hydrogen Energy* 46(39):20503–20515
42. Liu Q, Zhou Q, Gao C, Liu L, Ye H (2021) Excellent electrochemical stability of Co₃O₄ array with carbon hybridization derived from metal-organic framework. *Nanotechnology* 32(48):485710
43. Yang Y-L, Liu X-H, Hao M-Q, Zhang P-P (2015) Performance of a low-cost direct glucose fuel cell with an anion-exchange membrane. *International journal of hydrogen energy* 40(34):10979–10984
44. Wang L, Li M, Huang Z, Li Y, Qi S, Yi C, Yang B (2014) Ni–WC/C nanocluster catalysts for urea electrooxidation. *J Power Sources* 264:282–289
45. Ding Y, Zhang P, Zhuo Q, Ren H, Yang Z, Jiang Y (2011) A green approach to the synthesis of reduced graphene oxide nanosheets under UV irradiation. *Nanotechnology* 22(21):215601
46. Stobinski L, Lesiak B, Malolepszy A, Mazurkiewicz M, Mierzwa B, Zemek J, Jiricek P, Bieloshapka I (2014) Graphene oxide and reduced graphene oxide studied by the XRD, TEM and

- electron spectroscopy methods. *J Electron Spectrosc Relat Phenom* 195:145–154
47. Ban F, Majid SR, Huang NM, Lim H (2012) Graphene oxide and its electrochemical performance. *Int. J. Electrochem. Sci* 7(5):4345–4351
 48. Wang T, Zhang S, Yan X, Lyu M, Wang L, Bell J, Wang H (2017) 2-Methylimidazole-derived Ni–Co layered double hydroxide nanosheets as high rate capability and high energy density storage material in hybrid supercapacitors. *ACS applied materials & interfaces* 9(18):15510–15524
 49. Liang H, Lin J, Jia H, Chen S, Qi J, Cao J, Lin T, Fei W, Feng J (2018) Hierarchical NiCo-LDH/NiCoP@ NiMn-LDH hybrid electrodes on carbon cloth for excellent supercapacitors. *Journal of Materials Chemistry A* 6(31):15040–15046
 50. Cheng M, Yang R, Zhang L, Shi Z, Yang W, Wang D, Xie G, Shi D, Zhang G (2012) Restoration of graphene from graphene oxide by defect repair. *Carbon* 50(7):2581–2587
 51. Martin A, Escarpa A (2014) Graphene: the cutting-edge interaction between chemistry and electrochemistry. *TrAC, Trends Anal Chem* 56:13–26
 52. Tuinstra F, Koenig JL (1970) Raman spectrum of graphite. *The Journal of chemical physics* 53(3):1126–1130
 53. Farooqui U, Ahmad A, Hamid N (2018) Graphene oxide: a promising membrane material for fuel cells. *Renew Sustain Energy Rev* 82:714–733
 54. Chen J, Zheng H, Kang J, Yang F, Cao Y, Xiang M (2017) An alkaline direct oxidation glucose fuel cell using three-dimensional structural Au/Ni-foam as catalytic electrodes. *RSC Advances* 7(5):3035–3042
 55. Lemoine C, Dubois L, Napporn TW, Servat K, Kokoh KB (2020) Electrochemical energy conversion from direct oxidation of glucose on active electrode materials. *Electrocatalysis* 11(2):170–179
 56. Sakai H, Nakagawa T, Tokita Y, Hatazawa T, Ikeda T, Tsujimura S, Kano K (2009) A high-power glucose/oxygen biofuel cell operating under quiescent conditions. *Energy & Environmental Science* 2(1):133–138
 57. Chen J, Zhao CX, Zhi MM, Wang K, Deng L, Xu G (2012) Alkaline direct oxidation glucose fuel cell system using silver/nickel foams as electrodes. *Electrochimica acta* 66:133–138

Publisher's note Springer Nature remains neutral with regard to jurisdictional claims in published maps and institutional affiliations.